

Supplement of

Elevated Anthropogenic Contributions to Trace Elements in Marine Aerosols Compared to Coastal Qingdao in Eastern China

Yuxuan Qi et al.

Corresponding to: Yang Zhou (yangzhou@ouc.edu.cn)

Contents of this file

Texts S1 to S3

Figures S1 to S11

Tables S1 to S10

Supplemental Texts

Text S1: Quality assurance and quality control

(a) Trace elements

Assessment and implications of procedural blanks: Blank filters were processed and analyzed following the identical protocol to that of the samples. Average blank concentrations and standard deviations for all trace elements are summarized in Table S1. The impact of blanks was evaluated by quantifying their typical percentage fraction to the measured sample concentrations. For most elements, the blank fractions were below 10%. Among these, seven elements exhibited particularly low blank levels (<5%), with Fe blanks notably evaluated at 3.1% (marine samples) and 4.0% (Qingdao samples). Although the blank fractions for Al were higher in marine samples, it is crucial to note that all reported data have undergone rigorously blank-correction. Furthermore, Al was not included as an input species in our PMF source apportionment. With these measures, uncertainties due to filter blanks have been minimized and are not expected to influence the results considerably.

Digestion procedure and environmental control: The acid digestion of aerosol samples, including the evaporation to dryness step, was conducted inside a standard fume hood under ambient laboratory conditions. The following stringent measures were implemented to assess and mitigate potential contamination, especially critical for the low metal concentrations in cases of marine aerosols: (i) All sample processing steps were performed in parallel with procedural blank filters. (ii) All labware underwent rigorous acid cleaning: rinsed six times with Milli-Q water ($\geq 18.0 \text{ M}\Omega \cdot \text{cm}$), immersed in 20% HNO_3 bath for 24-hour, another six-time rinse with Milli-Q water, and finally dried in a clean bench. Filter samples were cut using a pre-cleaned ceramic knife and ceramic tweezers. (iii) All analytical results were blank-corrected using the procedural blanks. As evidenced by low blank levels for most elements, contamination introduced during the experimental process was effectively controlled and did not compromise data quality or the integrity of the scientific conclusions

(b) Water-soluble ions

Standard solutions were analyzed after every 10 samples to monitor instrumental precision and accuracy. Blank filters were analyzed at the same frequency to quantify and subtract any contamination introduced during the sample extraction process.

(c) Analysis of OC and EC

The concentrations of OC and EC were measured using a Sunset OC/EC analyzer (RT-3131, Sunset Laboratory, OR, USA). A 2.0 cm² punch of each quartz filter sample was analyzed following the National Institute for Occupational Safety and Health (NIOSH) 5040 thermal-optical transmittance (TOT) protocol.

The analysis involved a two-stage heating process. Initially, the punch sample was heated in a pure helium (He) atmosphere through a series of temperature steps to volatilize and quantify OC. During this stage, a portion of OC was pyrolyzed, forming pyrolyzed carbon (PC). Subsequently, the atmosphere was switched to a mixture of He and oxygen (He/O₂). In this oxidative environment, the sample was further heated, causing the remaining EC and the previously formed PC to combust. A critical correction for the PC formed during the He phase was applied. This was achieved by continuously monitoring the transmittance of a laser through the filter (Wu et al., 2016). The laser transmittance decreased as PC formed and recovered as PC and EC were combusted in the He/O₂ phase. The point at which the laser transmittance returns to its initial value is defined as the OC/EC split point. The carbon detected before this split point is defined as OC, and the carbon detected after is defined as EC. The carbonaceous gases produced in both stages were converted to carbon dioxide (CO₂) in a manganese dioxide (MnO₂) oxidation oven and then quantified by a flame ionization detector (FID) or a non-dispersive infrared (NDIR) detector.

The method detection limit is approximately 0.2 µgC m⁻³ for filter analysis, with an analytical uncertainty (standard deviation) between 4% and 6%. Obtained data were calibrated using a standard curve, and routine quality assurance includes the analysis of calibration standards and blank filters.

Text S2: Enrichment factor (EF) calculation

The EF was calculated to assess the anthropogenic influence on trace elements using Al as a reference element (R). The calculation followed the equation:

$$EF = \frac{(C_X/C_R)_{\text{aerosol}}}{(C_X/C_R)_{\text{crustal}}} \quad (1)$$

Where C_X is the concentration of element X in aerosols, C_R is the concentration of the reference element R in aerosols, and the denominator is the ratio of the content of element X to R in the Earth's crust. The crust values were taken from the upper continental crust composition reported by Taylor (1964).

Text S3: Detailed description of PMF analysis

Source contribution time series: The time series of individual PMF factor concentrations (e.g., Fig.4) were derived from the factor contributions output by the PMF model. A factor-specific scaling coefficient was calculated by

comparing the factor contribution and absolute concentration. The complete absolute concentration time series for each factor was then generated by applying this coefficient to the entire factor contribution time series.

PMF solution evaluation: Multiple factors ranging from 6 to 10 were thoroughly evaluated to determine the optimal solution. The stability and reliability of the factor solutions were assessed using the displacement (DISP) and bootstrap (BS) uncertainty estimation methods (Norris et al., 2014). Ultimately, an 8-factor solution emerged as the most robust and interpretable. In contrast, the 7-factor solution failed to distinguish the industrial emissions from dust (Fig.S1a). The 9-factor solution tended to resolve an additional factor; however, it exhibited relatively low BS mapping values (58%, 67%, and 73%) for several factors (Fig.S1b and Table S2). The 8-factor solution demonstrated the highest stability. The mapping percentages using the BS uncertainty method exceeded 80% for all factors (Table S3), surpassing the performances of the 7-factor and 9-factor solutions (Tables S4 and S2). Moreover, the DISP analysis showed no occurrences of factor swapping and no reduction in the model fit statistic Q (both %dQ and the error code were 0), further validating the stability and interpretation of the 8-factor solution.

Based on the established 8-factor PMF solution, a detailed evaluation of its performance in simulating Fe concentrations was conducted. The results showed that while the model performed well for most elements (e.g., Fig.S11b and c), the PMF-resolved total Fe in marine aerosols in summer (191.5 ng m^{-3}) was substantially higher than the measured concentration (109.8 ng m^{-3}), indicating an overestimation in the absolute source concentrations for Fe in this specific scenario. Therefore, the reported concentrations by PMF for marine Fe in summer should be interpreted as upper-bound estimates. Crucially, the strong linear correlation ($r^2 = 0.98$, $p < 0.01$) between the PMF-simulated and measured Fe concentrations ($r^2 = 0.76$, $p = 0.02$ for summer marine samples; Fig.S11a) indicated that the overestimation was proportional. This high coherence in temporal trends strongly suggested that the relative source contributions for Fe remained robust.

Supplemental Figures

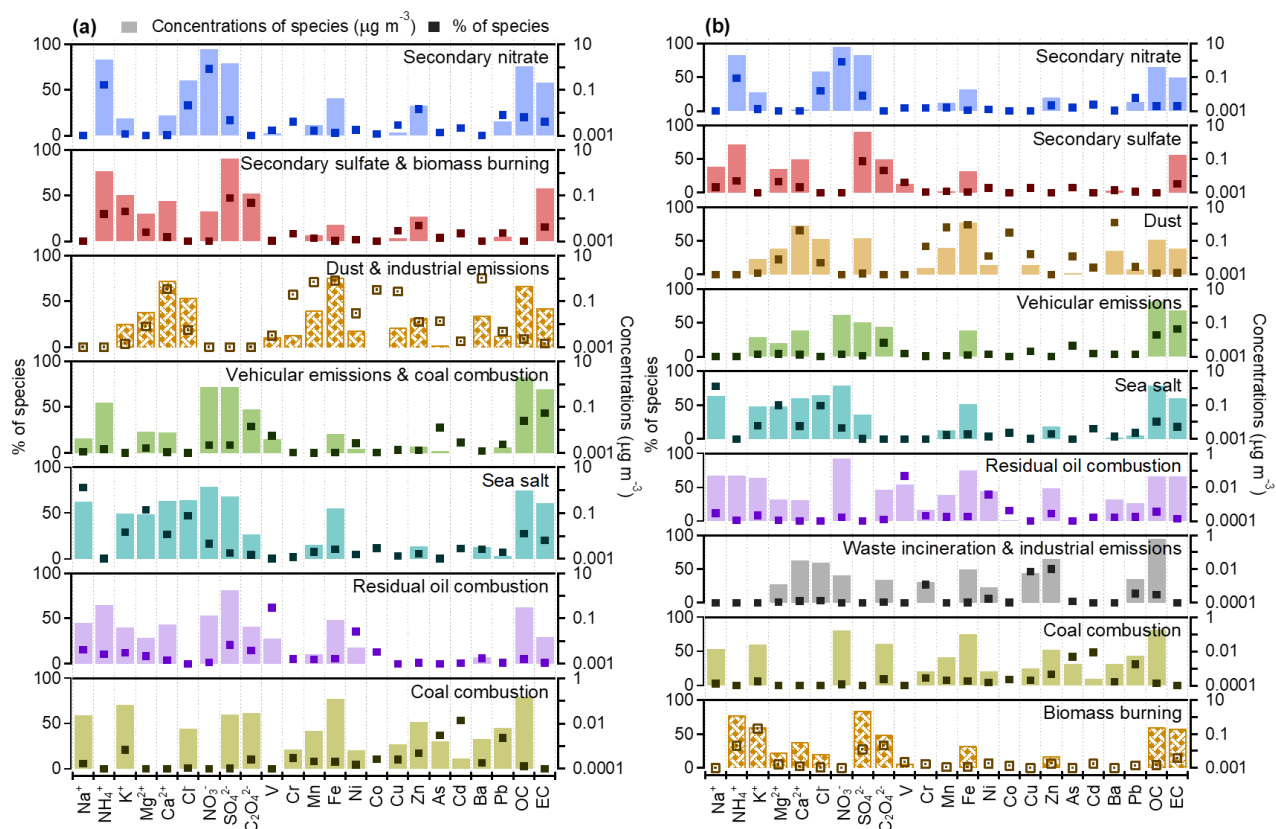


Figure S1: PMF resolved factor profiles (dark points represent the percentages and light rectangles represent the concentrations of each species in each factor) of (a) 7-factor and (b) 9-factor solution.

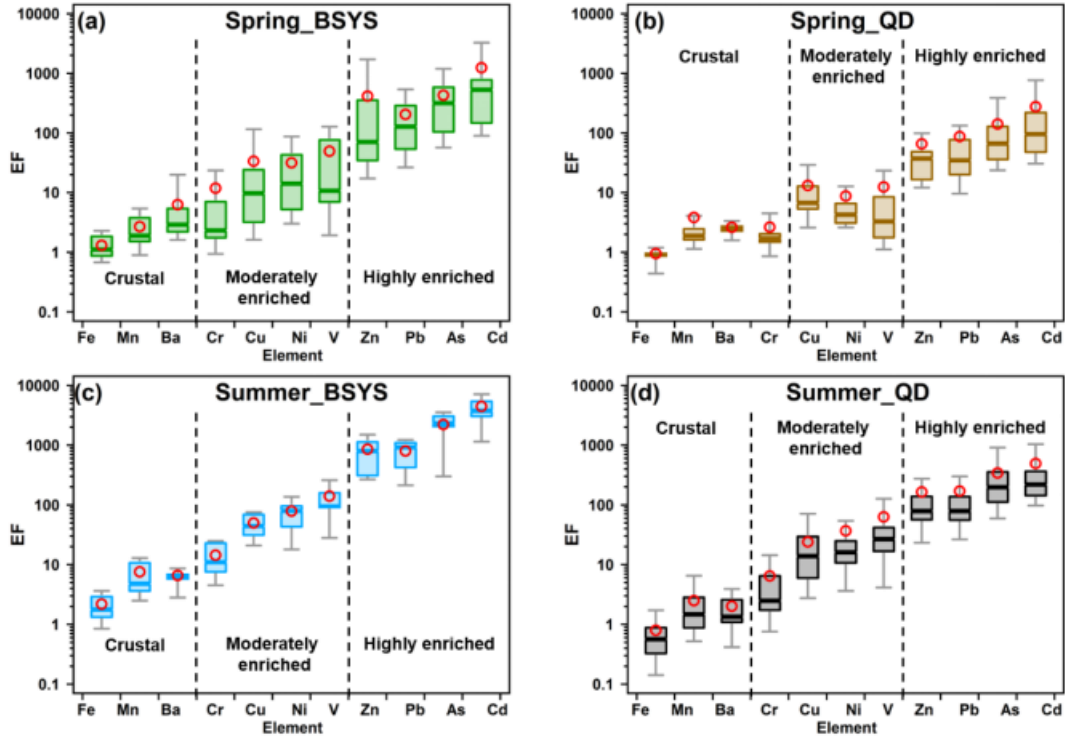


Figure S2: Elemental EFs in fine particles over (a) spring BS and YS, (b) spring QD, (c) summer BS and YS, and (d) summer QD. 25th and 75th percentile boxes; 10th and 90th percentile whiskers; the solid line is the median value, and the red circle is the mean value.

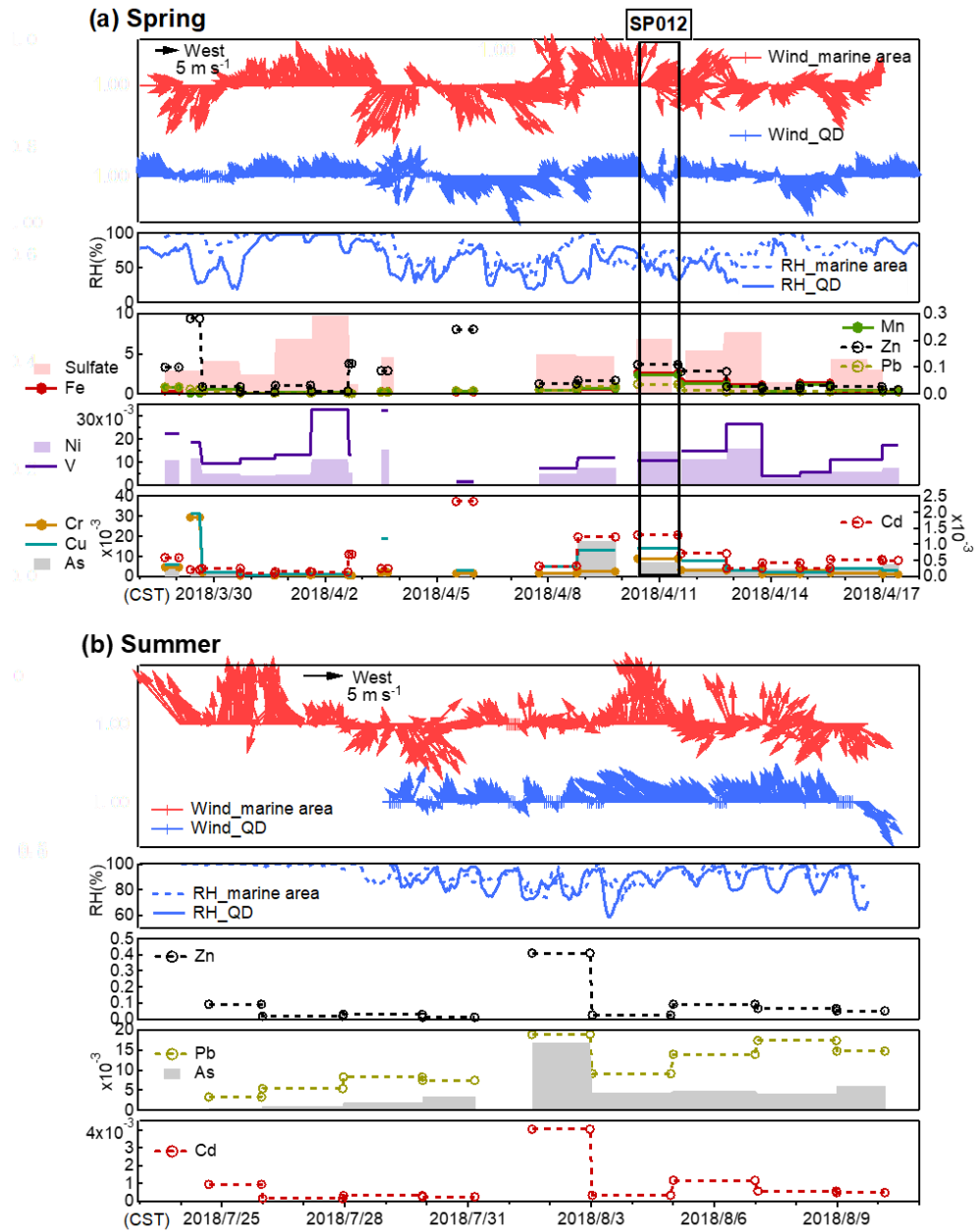


Figure S3. Temporal variations of meteorological parameters and selected species concentrations ($\mu\text{g m}^{-3}$) in (a) spring and (b) summer. “SP012” marked in (a) show the information about the sampling period for sample SP012. “Marine area” refers to the BS and YS.

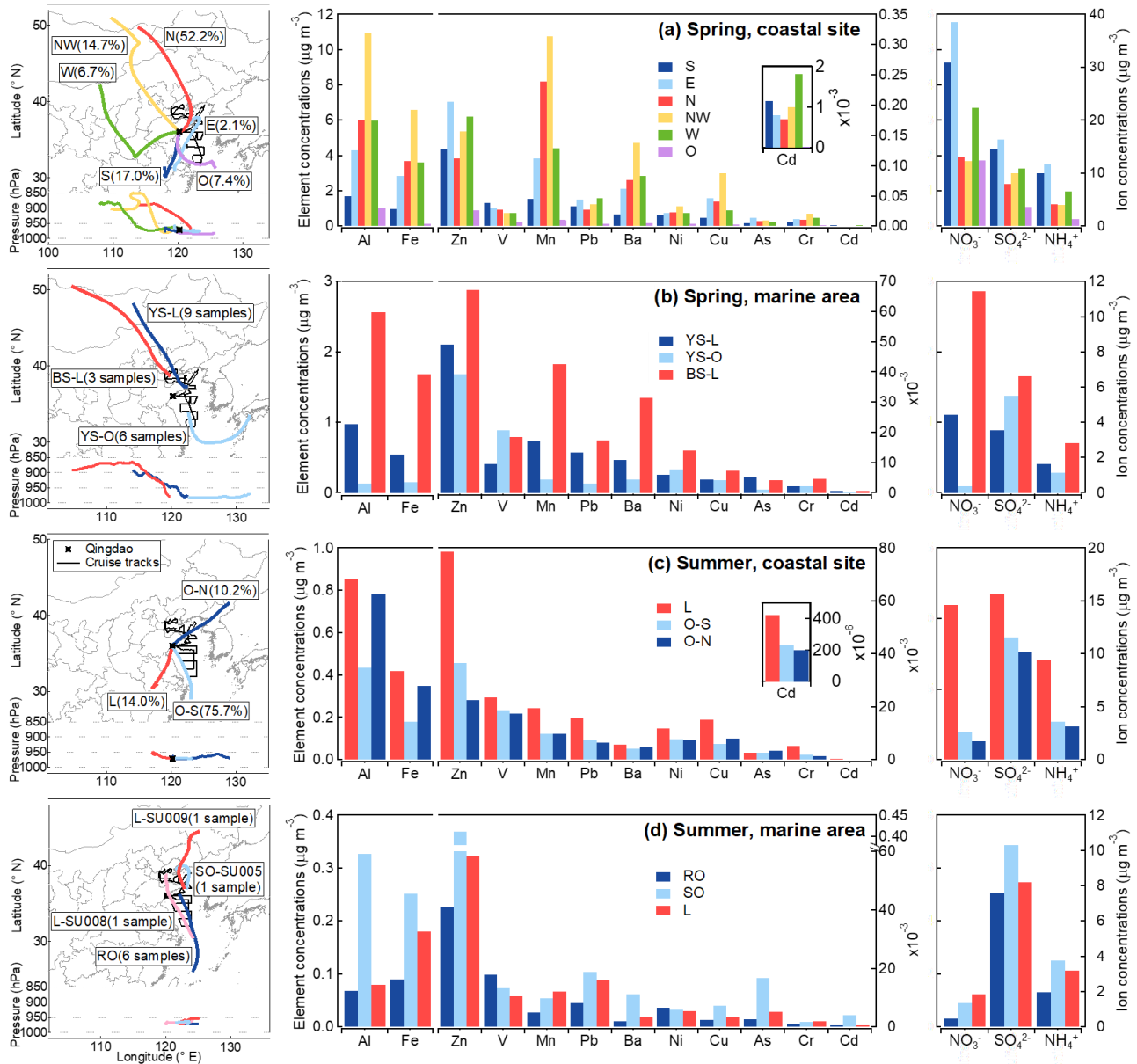


Figure S4. To explore the influence of air mass history on variations in trace element abundances, the backward trajectories calculated by HYSPLIT model were classified into six categories in spring and three in summer at the coastal city site (Qingdao), using a systematic clustering method implemented in the software SPSS (Statistical Product and Service Solutions) Statistics v21. For the cruise missions, the trajectory endpoints corresponded to the cruise coordinates, thus the samples were manually classified into three categories in both seasons. Averaged 72 h backward trajectories of air masses arriving at 300 m altitudes and the averaged concentrations of trace elements and ions of individual clusters in spring at (a) the coastal site (Qingdao) and (b) marine areas (BS and YS) and in summer at (c) the coastal site and (d) marine areas. The black star indicates the coastal site, Qingdao. The solid black line indicates the cruise tracks. “YS-O” means “YS-ocean”. Al and Fe use the left labels; other elements use

the right labels.

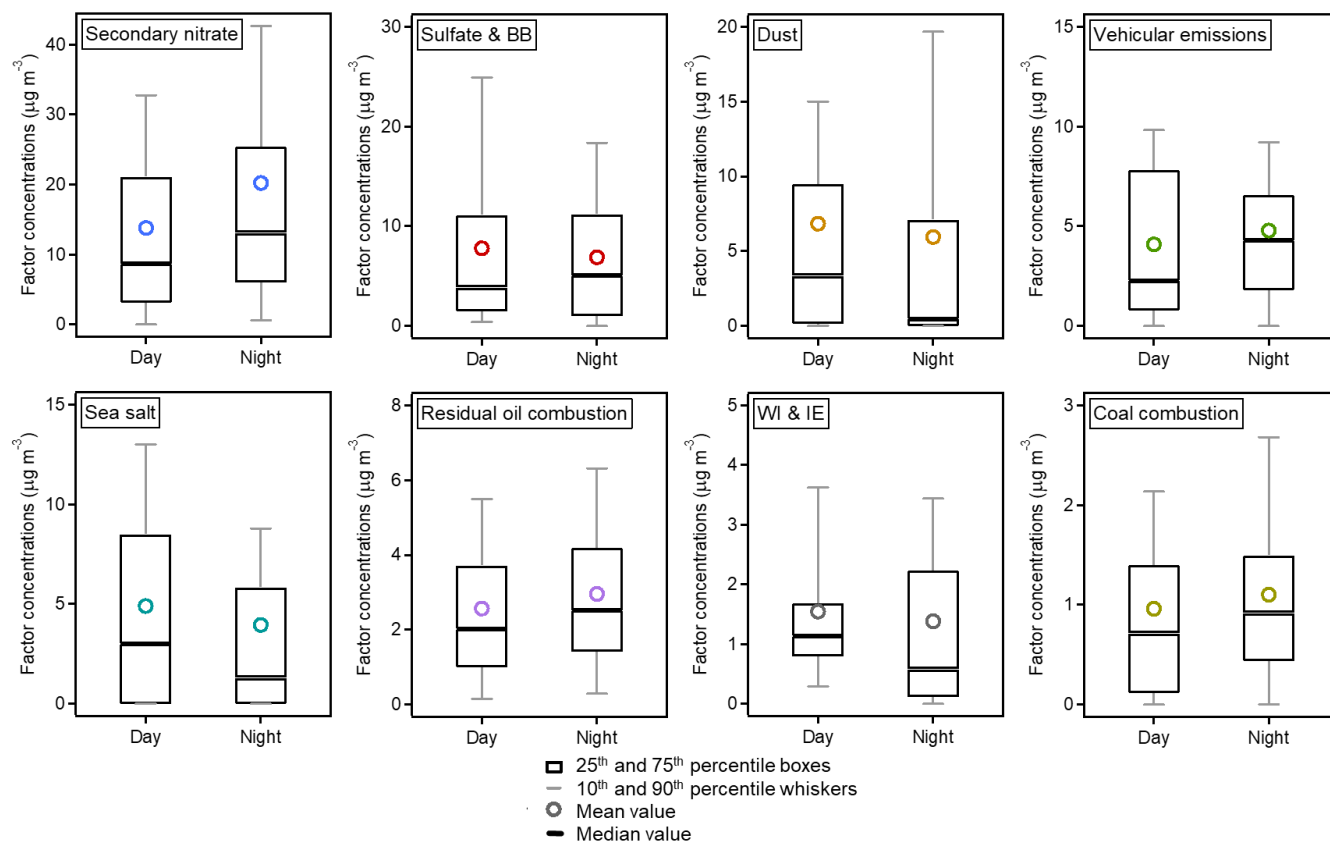


Figure S5. Diurnal variations of individual factor contributions from PMF results in Qingdao. (29 daytime and 26 nighttime samples were collected, respectively. 25th and 75th percentile boxes, 10th and 90th percentile whiskers; the solid black line is the median value, and the circle is the mean value.) Sulfate & BB represents sulfate & biomass burning. WI & IE represents waste incineration & industrial emissions.

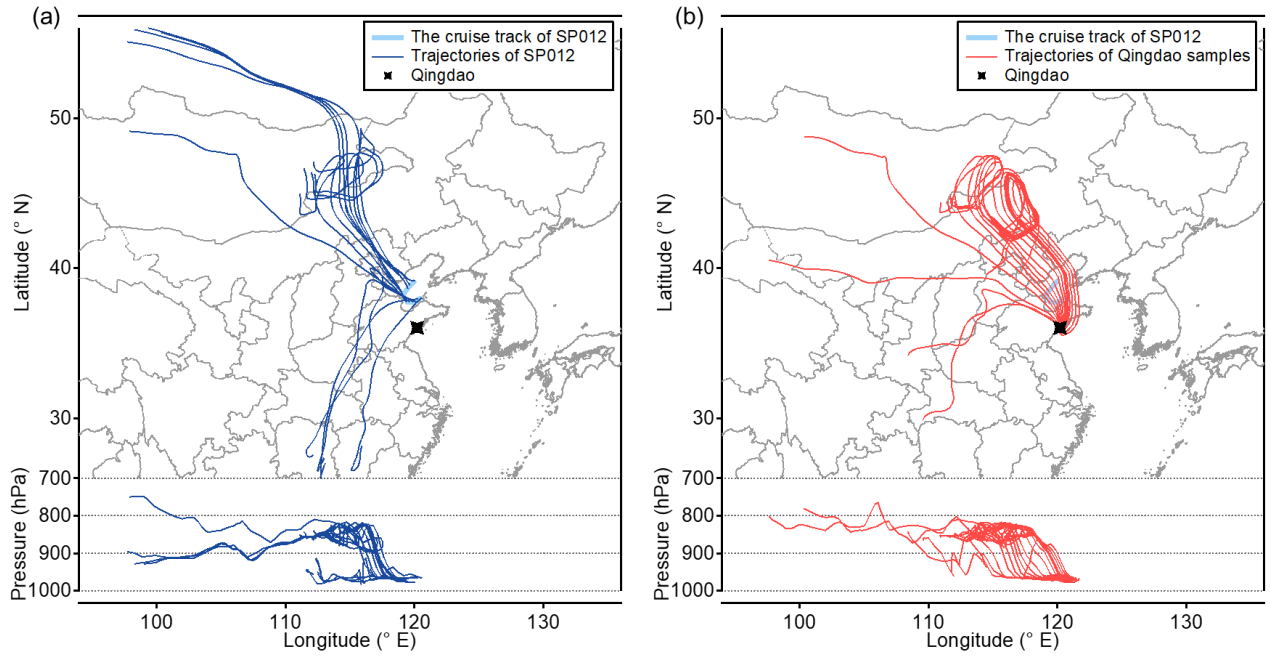


Figure S6. 72 h backward trajectories of air masses arriving 300 m altitude of (a) the marine sample SP012 and (b) its corresponding Qingdao samples.

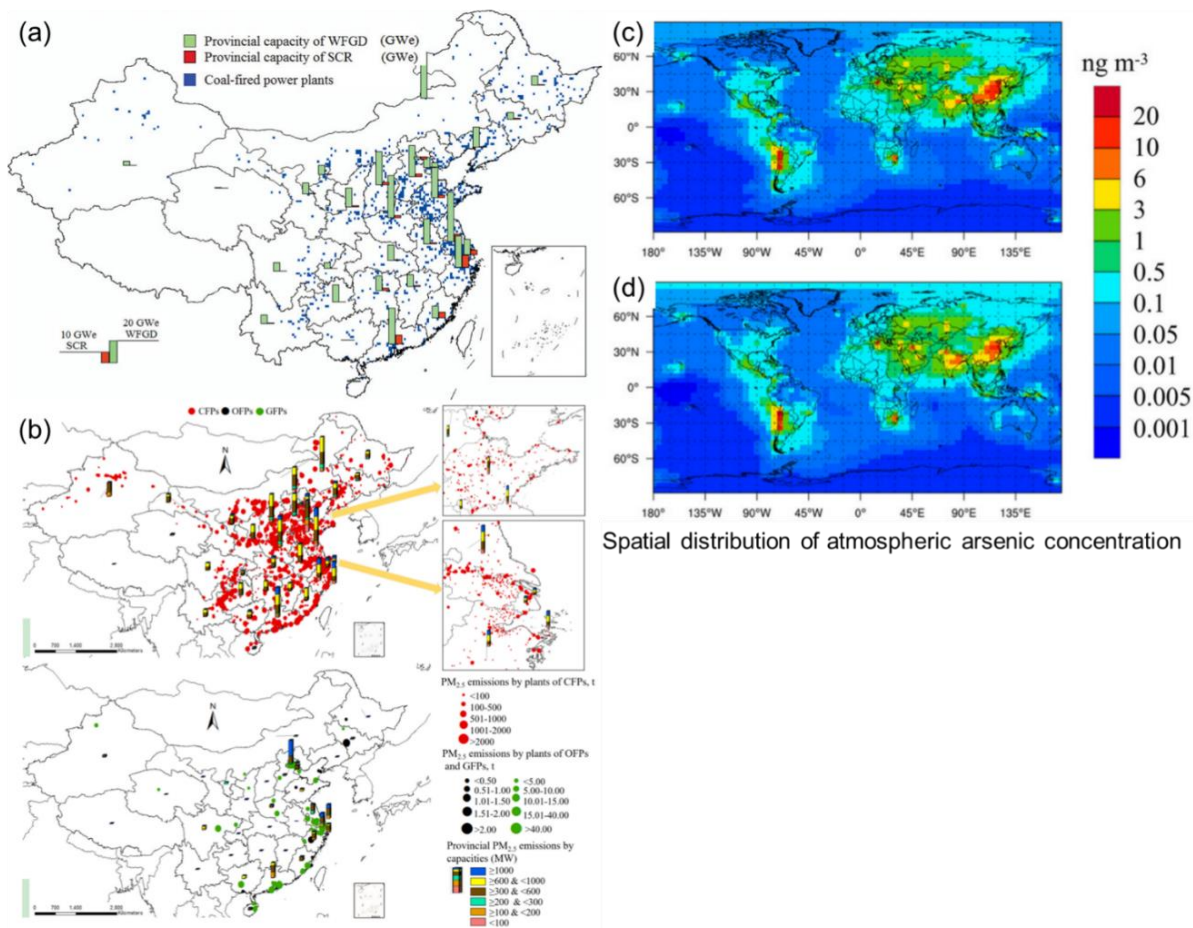
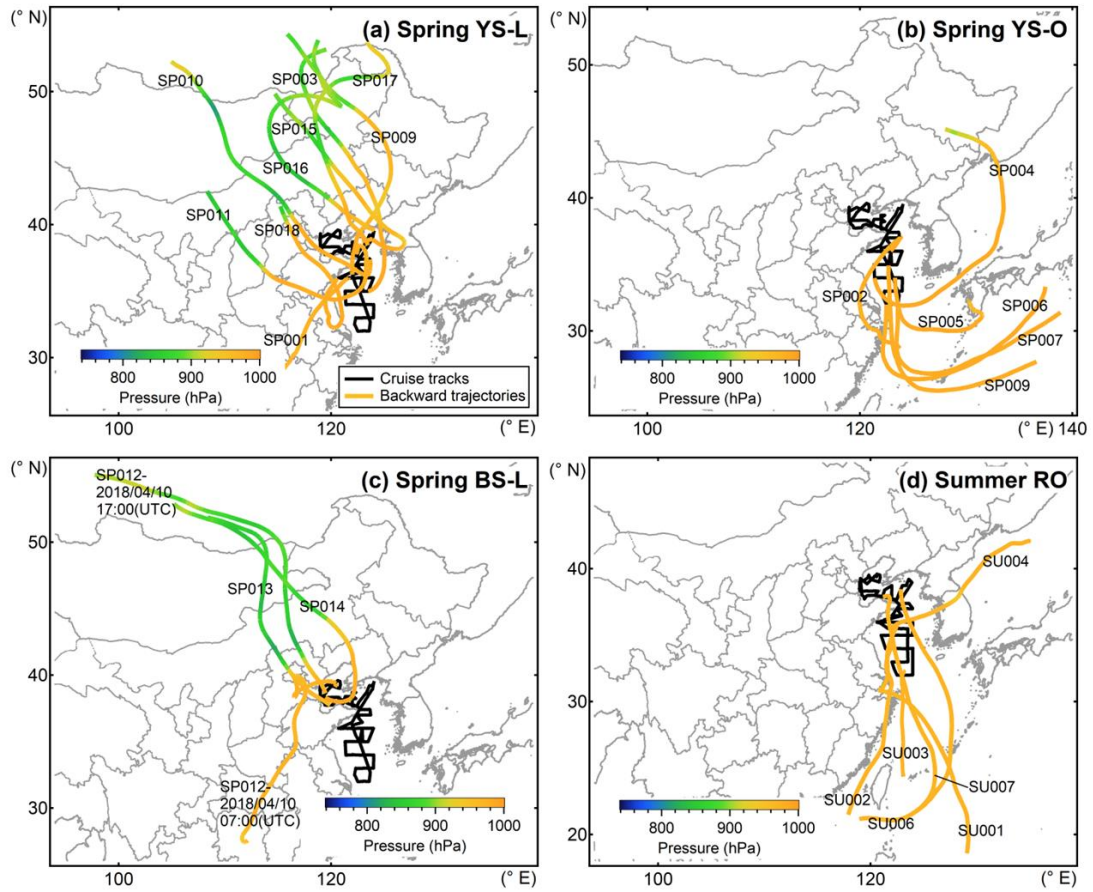


Figure S7. (a) Geographical distribution of coal-fired power plants in China, 2010 (Tian et al., 2014). WFGD represents wet flue gas desulfurization. SCR represents selective catalytic reduction. (b) Spatial distribution of PM_{2.5} emissions by coal-fired power plants in China, 2014 (Wang et al., 2016). CFPs, OFPs, and GFPs represent coal-fired power plants, oil-fired power plants, and natural gas-fired power plants, respectively. Spatial distribution of atmospheric arsenic (As) concentration from GEO-Chem in (c) 2005 and (d) 2015 (Zhang et al., 2020).



5962

Figure S8. Averaged 72 h backward trajectories arriving at the BS and YS in (a) (b) (c) spring and (d) summer of each sample. The black solid line indicates the cruise tracks. “YS-O” means “YS-ocean”.

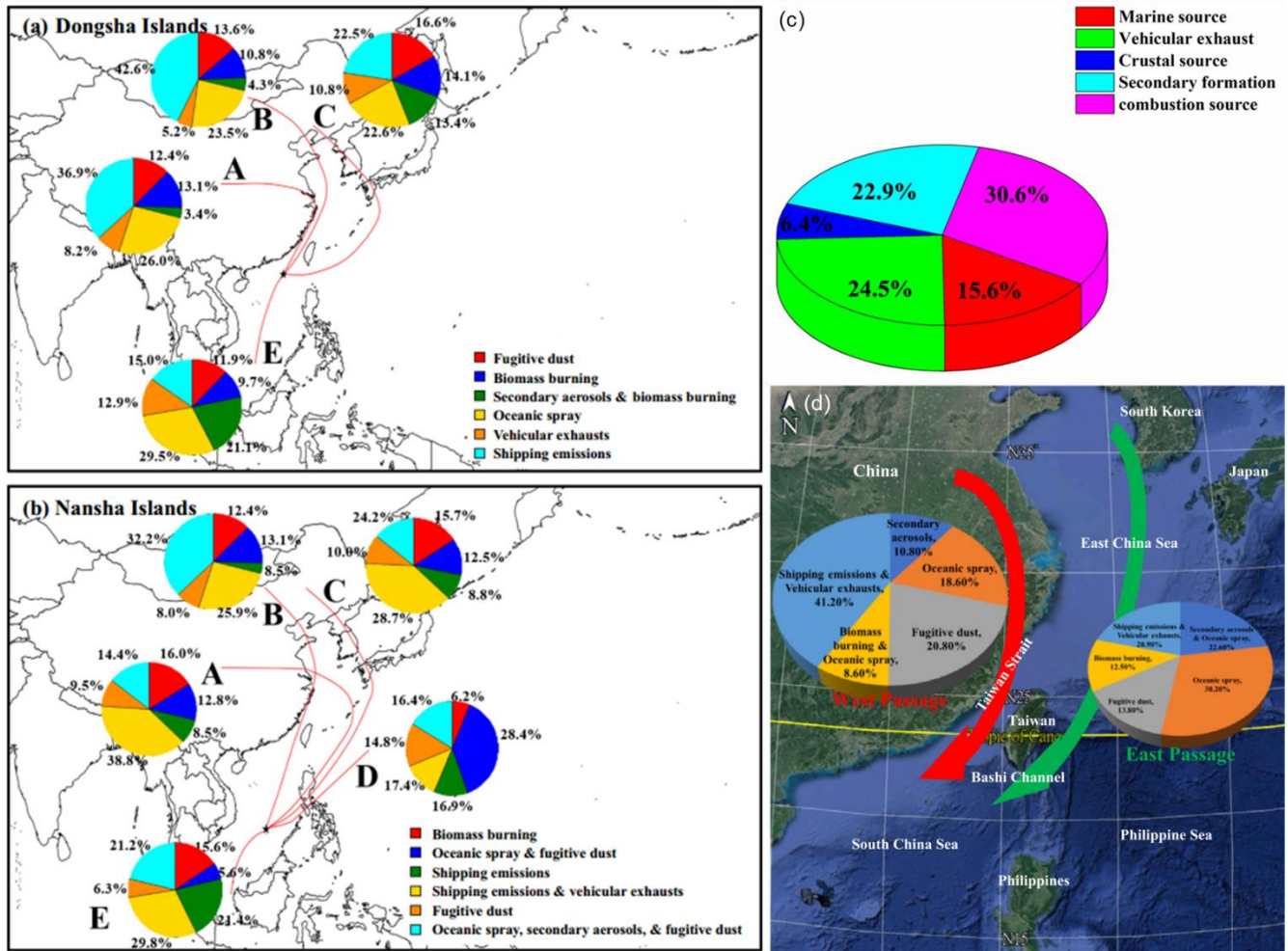


Figure S9. (a) Source contribution resolved from the PMF analysis of PM_{2.5} at (a) the Dongsha Islands and (b) the Nansha Islands for the transport route-based cluster analysis (A: Central China; B: North China; C: Korea, Japan, and Northeast China; D: the Philippines and the West Pacific Ocean; E: the South China Sea) (Yen et al., 2022b). (c) The contribution of different sources in PM_{2.5} in the Eastern China Sea (Sun et al., 2022). (d) Source apportionment of marine fine particles at two islands through the west and east passages of the Taiwan Island (Yen et al., 2022a).

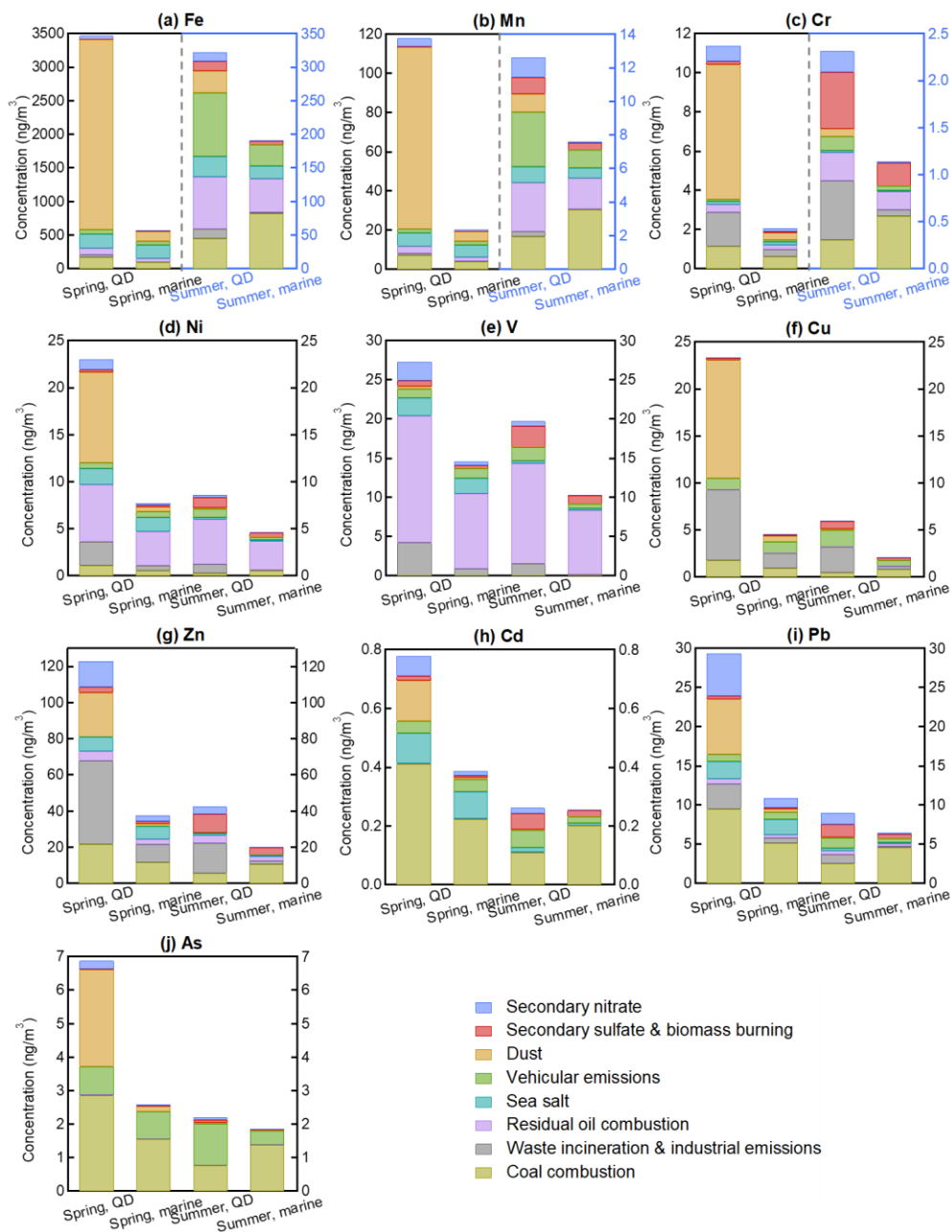


Figure S10. Concentrations of various source factors to individual elements based on PMF results. “marine” refers to the BS and YS. For Fe, Mn, and Cr, the left and right axes (spring vs. summer) use different scales, distinguished by color (right axis in blue).

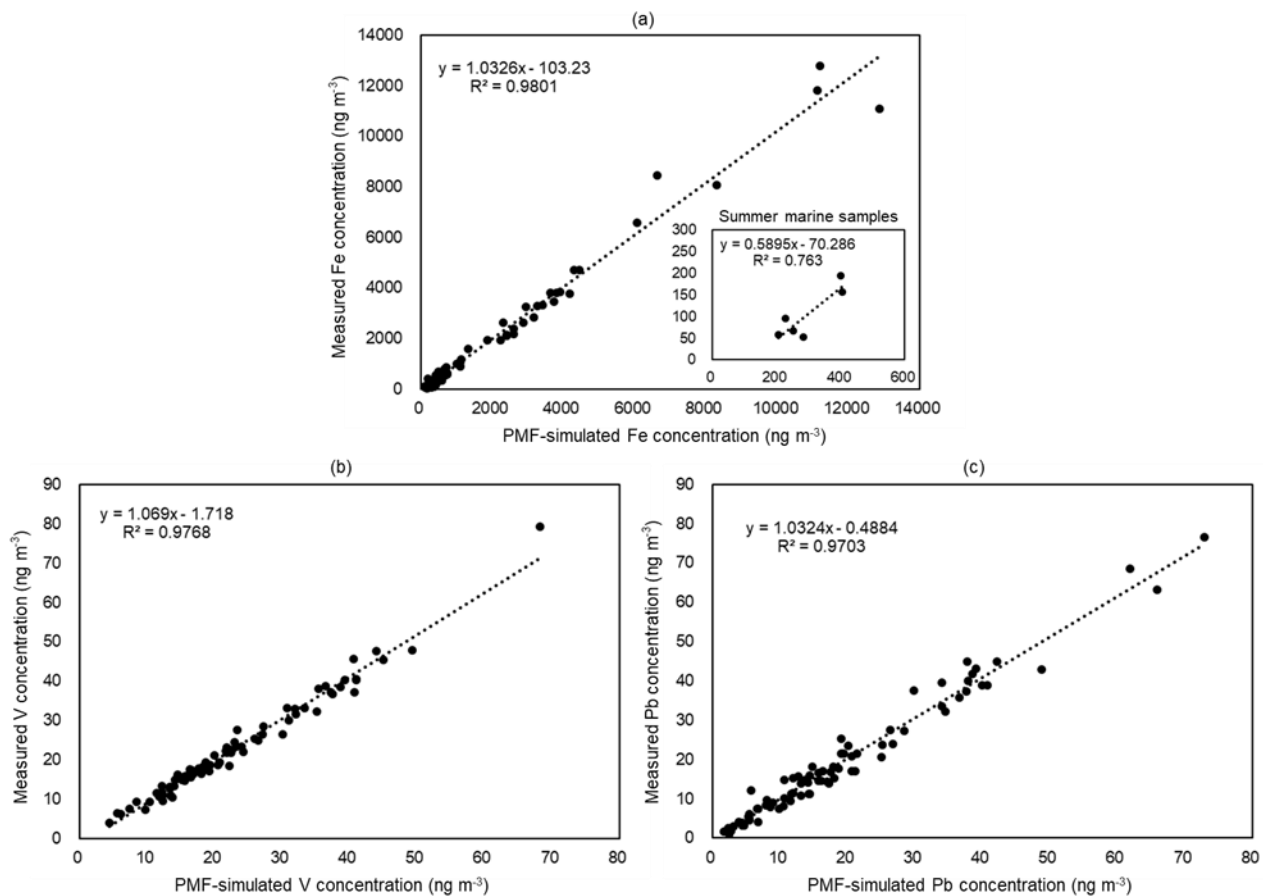


Figure S11. Comparison of measured and PMF-simulated concentrations (ng m^{-3}): (a) Fe, (b) V, and (c) Pb.

Table S4. BS mapping of 7-factor solution based on PMF.

	Base factor 1	Base factor 2	Base factor 3	Base factor 4	Base factor 5	Base factor 6	Base factor 7	Unmapped
Boot factor 1	80	5	3	1	1	3	2	5
Boot factor 2	0	100	0	0	0	0	0	0
Boot factor 3	5	6	79*	6	1	1	0	2
Boot factor 4	0	1	0	99	0	0	0	0
Boot factor 5	0	0	0	0	100	0	0	0
Boot factor 6	0	1	0	2	0	97	0	0
Boot factor 7	0	0	0	0	0	1	99	0

*. The mapping percentages were less than 80% using the BS uncertainty method.

Table S5. Comparison of concentrations (ng m^{-3}) of trace elements over the BS and YS in this study with other studies on $\text{PM}_{2.5}$ in oceanic regions of China.

Area	Time	Al	Fe	Zn	V	Mn	Pb	Ba	Ni	Cu	As	Cr	Cd	Reference
BS and YS	2018.3–4	1043.2	648.6	49.9	14.2	18.4	11.8	13.0	8.0	5.0	3.7	2.6	0.5	This study
	2018.7–8	71.1	109.8	44.9	16.2	6.5	9.9	2.3	6.4	2.6	3.2	1.4	0.5	
BS	2018.3–4	2562.8	1682.2	67.2	18.5	42.6	17.5	31.5	14.0	7.4	4.1	4.6	0.7	
	2018.7–8	72.6	162.3	79.7	13.1	9.6	15.5	2.9	5.8	3.0	4.6	1.9	0.9	
YS	2018.3–4	689.2	407.9	45.8	13.2	12.8	10.5	8.7	6.6	4.4	3.7	2.1	0.5	
	2018.7–8	70.5	92.7	33.6	17.3	5.5	8.0	2.1	6.5	2.4	2.8	1.2	0.4	
YS	2011.3–4	2803.3	1111.8	74.2	20.7	14.8	18.9	-	20.1	11.5	8.6	-	-	Zhao et al., 2015
ECS	2018.4–5	244.1	223.0	37.9	22.4	10.5	10.6	8.5	8.9	8.0	3.8	14.7	0.3	Sun et al., 2022
Pengjiayu, ECS*	2019.9– 2020.8	109.9	71.7	5.7	0.6	1.9	1.5	-	0.4	-	-	-	0.1	Hsieh et al., 2023
Huaniao Island, ECS**	2015–2018	-	160.0	-	-	-	-	-	-	-	-	-	-	Yang et al., 2020
Penghu Islands (PH)	2017.8–9	150	180	40	20	30	40	-	10	20	-	20	<5	Yuan et al., 2023
Dongsha Islands (DS)		80	70	50	<5	10	20	-	<5	20	-	10	<5	
Nansha Islands (NS)***		50	50	30	<5	<5	<5	-	<5	20	-	10	<5	
PH	2018.3–4	450	370	150	80	40	100	-	70	30	-	50	30	
DS		360	310	120	60	30	80	-	60	30	-	40	30	
NS		60	70	40	10	10	50	-	20	10	-	20	20	

*. The data in this study were derived from particles with aerodynamic diameters less than $3.1 \mu\text{m}$ ($\text{PM}_{3.1}$).

** . The data in this study were derived from particles with aerodynamic diameters less than $1.8 \mu\text{m}$ ($\text{PM}_{1.8}$).

*** . The three remote islands (PH, DS, and NS) were located from the south Taiwan Strait (TS) to the north South China Sea (SCS).

Table S6. Comparison of concentrations (ng m^{-3}) of trace elements in Qingdao in this study with other studies on $\text{PM}_{2.5}$ in typical cities of China.

City	Type	Time	Al	Fe	Zn	V	Mn	Pb	Ba	Ni	Cu	As	Cr	Cd	Reference
Qingdao	Coastal	2018.3–4	5573.5	3347.3	120.1	26.4	127.8	29.3	70.3	21.9	39.5	7.6	11.1	0.8	This study
		2018.7–8	572.9	228.3	40.9	19.2	11.1	8.6	4.4	8.3	7.4	2.7	2.4	0.3	
Qingdao	Coastal	2018.6–7	548.9	347.3	91.7	9.4	~11	22.5	~11	-	-	-	-	-	Li et al., 2018
Qingdao*	Coastal	2019.11–12	935.5	801.0	57.1	2.3	29.9	14.9	19.2	2.5	43.5	2.5	4.3	0.5	Zhang et al., 2021
Beijing	Inland	2005.3–2006.2	790	1130	530	30	90	240	210	20	70	20	50	50	Chen et al., 2008
Tianjin	Coastal	2017.10–2018.8	-	409	136	2	20	31	-	12	33	18	-	-	Zhang et al., 2021
Shanghai	Coastal	2016.3–2017.2	-	410	120	13	32	27	24	6	12	6.6	4.5	9.6	Chang et al., 2018
Shanghai**	Coastal	2004.4–2005.4	-	950	349	9	51	143	12	8	29	28	15	3.7	Chen et al., 2008
Ningbo	Coastal	2014.3–5	1430	1420	229	9.4	-	68.9	-	10.0	20.1	-	14.1	-	Ming et al., 2017
		2014.6–8	676	354	65.3	3.2	-	14.7	-	4.0	4.6	-	9.3	-	
Xiamen	Coastal	2017.1–2018.1	210	290	86.7	10.6	14.3	19.3	11.3	7.1	7.2	1.6	8.5	0.5	Wu et al., 2020
Guangzhou	Coastal	2008.12–2009.2	-	1850	1360	20	150	450	70	-	190	40	70	20	Yang et al., 2011
Hangzhou**	Near-coastal	2018.11–2020.1	2194.4	2529.1	160.4	2.8	33.2	36.0	59.9	22.1	46.1	-	21.2	-	Zhu et al., 2022

*. The data in this study were derived from particles with aerodynamic diameters less than $1 \mu\text{m}$ (PM_{1}).

** . An urban-residential site, Putuo.

***. The data were obtained from the analysis using an energy dispersive X-ray fluorescence (EDXRF) spectrometer ($\text{in } \mu\text{g cm}^{-2}$) and have been converted by the authors of this study (in ng m^{-3}).

Table S7. Pearson correlations (r) of PMF factor contributions with meteorological parameters (relative humidity (RH) and wind speed (WS)), and gas pollutants concentrations (SO₂, NO₂, O₃ and CO).

Factor	RH	WS	SO ₂	NO ₂	O ₃	CO
Secondary nitrate	-0.18	-0.17	0.30*	0.45**	0.26*	0.39**
Secondary sulfate & biomass burning	0.36**	-0.25*	-0.46**	-0.52**	0.39**	0.54**
Dust	-0.72**	0.18	0.19	0.35**	-0.13	-0.13
Dust (spring, coastal)	-	0.43*	-	-	-	-
Vehicular emissions	0.01	-0.36**	0.11	0.10	-0.37**	0.30*
Vehicular emissions (summer)	-	-	-	0.78**	-	-
Sea salt	-0.63**	0.35**	0.31*	0.46**	-0.05	-0.03
Residual oil combustion	0.06	-0.24*	0.38**	0.19	-0.06	-0.05
Waste incineration & Industrial emissions	-0.33**	0.10	0.31*	0.50**	-0.06	0.24
Coal combustion	-0.23*	0.00	0.35**	0.54**	0.18	0.27*

Note. The highest correlation coefficients for each factor are denoted in bold. No gas pollutants data was available for the cruise campaign. The meteorological parameters of the former eight samples in summer Qingdao are missing values.

*. Correlation is significant at the 0.05 level (2-tailed).

**. Correlation is significant at the 0.01 level (2-tailed).

Table S8. The information of averaged 72 h air mass backward trajectory clusters arriving at the coastal site (Qingdao) and marine area (BS and YS) in spring and summer.

Campaign	Cluster	Detailed information	Frequency
Spring, coastal site	N (North)	From the north and passed the Inner Mongolia Autonomous region and Liaoning Province	52.2%
	NW (Northwest)	From the northwest and passed the Inner Mongolia Autonomous and BTH region	14.7%
	W (West)	From the Inner Mongolia Autonomous region and passed Shaanxi and Henan Provinces	6.7%
	S (South)	From East China near the Yangtze River Delta (YRD)	17.0%
	E (East)	From East China near YRD and passed YS before reversing to the Shandong Peninsula	2.1%
	O (Ocean)	Mainly from ECS and passed YS	7.4%
Spring, marine area	BS-L (BS-Land)	BS samples influenced by the continent air masses	Three samples
	YS-L (YS-Land)	YS samples influenced by the continent air masses	Nine samples
	YS-O (YS-Ocean)	YS samples influenced by the marine air masses	Six samples
Summer, coastal site	L (Land)	Passed the continent of East China before arriving at QD	14.0%
	O-S (Ocean-South)	From ECS in the south	75.7%
	O-N (Ocean-North)	From Korean Peninsula in the north	10.2%
Summer, marine area	L (Land)	Two samples influenced by the continent air masses, one passed the coastline of southeastern China (L-SU008), another from the northern China (L-SU009)	Two samples
	RO (Remote oceans)	Samples influenced by remote ocean air masses	Six samples
	SO (Surrounding oceans)	BS sample influenced by the air masses lingered over the CBS region	One sample, SU005

Table S9. Percentage contributions (%) of various source factors to individual elements based on PMF. “Marine” refers to the BS and YS areas, while “coastal” refers to Qingdao, hereinafter the same.

Element	Season	location	Secondary nitrate	Sulfate & BB	Dust	VE	Sea salt	ROC	WI & IE	CC
Fe	Spring	Coastal	1.4	0.1	81.6	1.8	6.1	2.8	1.1	4.9
		Marine	1.9	0.3	25.4	11.0	33.6	10.2	1.4	16.2
	Summer	Coastal	4.3	4.3	10.3	29.1	9.5	24.1	4.3	14.1
		Marine	0.6	2.9	-	16.7	9.8	26.1	0.8	43.2
Mn	Spring	Coastal	3.6	0.2	78.6	1.8	5.7	3.1	0.8	6.2
		Marine	4.5	0.7	23.4	10.6	29.7	10.7	0.9	19.5
	Summer	Coastal	9.3	7.9	8.6	25.7	7.6	22.9	2.6	15.4
		Marine	1.2	5.2	-	14.4	7.7	24.4	0.5	46.5
Cr	Spring	Coastal	7.1	1.5	60.4	0.9	1.5	3.3	15.3	10.1
		Marine	8.2	4.2	16.9	4.8	7.5	10.6	17.7	30.0
	Summer	Coastal	9.5	26.1	3.5	6.5	1.1	12.8	27.3	13.3
		Marine	1.5	21.1	-	4.4	1.3	16.6	5.9	49.1
Ni	Spring	Coastal	4.6	1.3	41.9	2.6	7.5	26.2	11.2	4.7
		Marine	2.9	2.1	6.4	7.7	20.2	46.2	7.1	7.5
	Summer	Coastal	3.4	12.7	1.3	10.3	2.9	55.2	10.8	3.3
		Marine	0.5	9.5	-	6.6	3.3	66.6	2.2	11.3
V	Spring	Coastal	8.7	2.7	1.1	4.4	8.2	59.4	15.5	-
		Marine	3.5	2.6	0.1	8.1	13.8	65.7	6.2	-
	Summer	Coastal	3.3	13.5	0.0	9.0	1.6	64.8	7.8	-
		Marine	0.5	10.3	-	5.9	1.9	79.8	1.6	-
Cu	Spring	Coastal	-	1.0	54.0	5.2	-	-	32.2	7.6
		Marine	-	2.6	14.3	26.5	-	-	35.3	21.3
	Summer	Coastal	-	13.8	2.5	30.1	-	-	45.7	7.9
		Marine	-	15.7	-	29.2	-	-	13.9	41.2
Zn	Spring	Coastal	11.7	2.4	20.2	-	6.4	4.2	37.5	17.7
		Marine	8.2	4.0	3.4	-	18.8	8.1	26.0	31.5
	Summer	Coastal	9.3	24.7	0.7	-	2.6	9.6	39.4	13.7
		Marine	1.6	20.7	-	-	3.4	12.9	8.8	52.5
Cd	Spring	Coastal	8.8	1.9	17.6	5.2	13.2	0.3	-	53.0
		Marine	3.8	2.0	1.8	10.3	23.9	0.3	-	57.8
	Summer	Coastal	7.2	20.9	0.6	22.9	5.6	0.7	-	42.1
		Marine	0.6	8.6	-	8.0	3.6	0.4	-	78.8
Pb	Spring	Coastal	18.4	1.5	23.9	3.1	7.6	2.1	10.9	32.5
		Marine	10.6	2.1	3.3	8.3	18.5	3.4	6.2	47.6
	Summer	Coastal	16.5	17.5	0.9	15.0	3.6	5.4	12.8	28.3
		Marine	1.8	9.7	-	7.1	3.0	4.9	1.9	71.6
As	Spring	Coastal	3.5	0.3	41.9	12.3	-	-	0.5	41.5
		Marine	2.0	0.5	5.7	31.9	-	-	0.3	59.7
	Summer	Coastal	3.0	3.7	1.5	56.6	-	-	0.5	34.6
		Marine	0.3	1.8	-	22.8	-	-	0.1	75.0

Note. Sulfate & BB represents sulfate & biomass burning. VE represents vehicular emissions. ROC represents residual oil combustion. WI & IE represents waste incineration & industrial emissions. CC represents coal combustion. A dash (-) indicates that the species is entirely absent from the factor profile for that period, not that its concentration is rounded to zero, hereinafter the same.

Table S10. Concentrations (ng m⁻³) of various source factors to individual elements based on PMF.

Element	Season	location	Secondary nitrate	Sulfate & BB	Dust	VE	Sea salt	ROC	WI & IE	CC
Fe	Spring	Coastal	50.12	3.80	2832.00	63.72	212.82	98.67	38.36	170.19
		Marine	10.72	1.99	145.19	62.62	191.58	58.26	8.14	92.36
	Summer	Coastal	13.73	13.76	33.33	94.03	30.60	77.79	13.92	45.46
		Marine	1.11	5.49	-	31.90	18.75	50.02	1.48	82.77
Mn	Spring	Coastal	4.29	0.28	92.73	2.20	6.70	3.67	0.89	7.30
		Marine	0.92	0.14	4.75	2.16	6.03	2.17	0.19	3.96
	Summer	Coastal	1.17	1.00	1.09	3.24	0.96	2.89	0.32	1.95
		Marine	0.09	0.40	-	1.10	0.59	1.86	0.03	3.55
Cr	Spring	Coastal	0.80	0.17	6.88	0.10	0.17	0.37	1.74	1.15
		Marine	0.17	0.09	0.35	0.10	0.16	0.22	0.37	0.63
	Summer	Coastal	0.22	0.60	0.08	0.15	0.02	0.30	0.63	0.31
		Marine	0.02	0.24	-	0.05	0.02	0.19	0.07	0.56
Ni	Spring	Coastal	1.06	0.30	9.63	0.60	1.73	6.04	2.58	1.07
		Marine	0.23	0.16	0.49	0.59	1.56	3.57	0.55	0.58
	Summer	Coastal	0.29	1.10	0.11	0.89	0.25	4.76	0.96	0.29
		Marine	0.02	0.44	-	0.30	0.15	3.06	0.10	0.52
V	Spring	Coastal	2.37	0.74	0.31	1.21	2.23	16.23	4.23	-
		Marine	0.51	0.38	0.02	1.18	2.01	9.58	0.90	-
	Summer	Coastal	0.65	2.66	0.00	1.78	0.32	12.80	1.54	-
		Marine	0.05	1.06	-	0.60	0.20	8.23	0.16	-
Cu	Spring	Coastal	-	0.23	12.59	1.22	-	-	7.51	1.77
		Marine	-	0.12	0.64	1.20	-	-	1.59	0.96
	Summer	Coastal	-	0.82	0.15	1.80	-	-	2.73	0.47
		Marine	-	0.33	-	0.61	-	-	0.29	0.86
Zn	Spring	Coastal	14.36	2.90	24.79	-	7.83	5.16	46.12	21.82
		Marine	3.07	1.52	1.27	-	7.05	3.05	9.79	11.84
	Summer	Coastal	3.93	10.50	0.29	-	1.13	4.07	16.74	5.83
		Marine	0.32	4.19	-	-	0.69	2.62	1.78	10.61
Cd	Spring	Coastal	0.07	0.02	0.17	0.04	0.10	0.00	-	0.41
		Marine	0.01	0.01	0.01	0.04	0.09	0.00	-	0.22
	Summer	Coastal	0.02	0.05	0.00	0.06	0.01	0.00	-	0.11
		Marine	0.00	0.02	-	0.02	0.01	0.00	-	0.20
Pb	Spring	Coastal	5.41	0.43	7.02	0.92	2.24	0.62	3.19	9.53
		Marine	1.16	0.23	0.36	0.90	2.01	0.37	0.68	5.17
	Summer	Coastal	1.48	1.57	0.08	1.35	0.32	0.49	1.16	2.55
		Marine	0.12	0.63	-	0.46	0.20	0.31	0.12	4.64
As	Spring	Coastal	0.24	0.02	2.88	0.84	-	-	0.03	2.86
		Marine	0.05	0.01	0.15	0.83	-	-	0.01	1.55
	Summer	Coastal	0.07	0.08	0.03	1.25	-	-	0.01	0.76
		Marine	0.01	0.03	-	0.42	-	-	0.00	1.39

Note. Sulfate & BB represents sulfate & biomass burning. VE represents vehicular emissions. ROC represents residual oil combustion. WI & IE represents waste incineration & industrial emissions. CC represents coal combustion. Absolute source concentrations are reported with two decimal places to accurately represent low concentration values and to avoid reporting 0.0 ng m⁻³ for non-zero concentrations. This provides a more precise dataset for reference. The main text adheres to the one-decimal-place convention for consistency in presentation.

References

- Chang, Y., Huang, K., Xie, M., Deng, C., Zou, Z., Liu, S., and Zhang, Y.: First long-term and near real-time measurement of trace elements in China's urban atmosphere: Temporal variability, source apportionment and precipitation effect. *Atmos. Chem. Phys.*, 18, 11793-11812. <https://doi.org/10.5194/acp-18-11793-2018>, 2018.
- Chen, J., Tan, M., Li, Y., Zheng, J., Zhang, Y., Shan, Z., Zhang, G., and Li, Y.: Characteristics of trace elements and lead isotope ratios in PM_{2.5} from four sites in Shanghai, *J. Hazard. Mater.*, 156, 36-43, <https://doi.org/10.1016/j.jhazmat.2007.11.122>, 2008.
- Hsieh, C. -C., You, C. -F., & Ho, T. -Y.: The solubility and deposition flux of East Asian aerosol metals in the East China Sea: The effects of aeolian transport processes. *Mar. Chem.*, 253, 104268. <https://doi.org/10.1016/j.marchem.2023.104268>, 2023.
- Li, P., Li, Q., Shi, J., Gao, H., and Yao, X.: Concentration, solubility, and dry deposition flux of trace elements in fine and coarse particles in Qingdao during summer (in Chinese), *Environ. Sci.*, 39, 3067-3074, <https://doi.org/10.13227/j.hjkk.201712231>, 2018.
- Ming, L., Jin, L., Li, J., Fu, P., Yang, W., Liu, D., Zhang, G., Wang, Z., and Li, X.: PM_{2.5} in the Yangtze River Delta, China: Chemical compositions, seasonal variations, and regional pollution events. *Environ. Pollut.*, 223, 200-212, <https://doi.org/10.1016/j.envpol.2017.01.013>, 2017.
- Sun, H., Sun, J., Zhu, C., Yu, L., Lou, Y., Li, R., and Lin, Z.: Chemical characterizations and sources of PM_{2.5} over the offshore Eastern China sea: Water soluble ions, stable isotopic compositions, and metal elements. *Atmos. Pollut. Res.*, 13, 101410, <https://doi.org/10.1016/j.apr.2022.101410>, 2022.
- Taylor, S. R.: Trace element abundances and the chondritic earth model, *Geochim. Cosmochim. Ac.*, 28, 1989-1998, [https://doi.org/10.1016/0016-7037\(64\)90142-5](https://doi.org/10.1016/0016-7037(64)90142-5), 1964.
- Tian, H., Liu, K., Zhou, J., Lu, L., Hao, J., Qiu, P., Gao, J., Zhu, C., Wang, K., and Hua, S.: Atmospheric Emission Inventory of Hazardous Trace Elements from China's Coal-Fired Power Plants-Temporal Trends and Spatial Variation Characteristics, *Environ. Sci. Technol.*, 48, 3575-3582, <http://doi.org/10.1021/es404730j>, 2014.
- Wang, Y., Cheng, K., Tian, H.-Z., Yi, P., and Xue, Z.-G.: Emission Characteristics and Control Prospects of Primary PM_{2.5} from Fossil Fuel Power Plants in China, *Aerosol Air Qual. Res.*, 16, 3290-3301, <http://doi.org/10.4209/aaqr.2016.07.0324>, 2016.
- Wu, C., Huang, X. H. H., Ng, W., Griffith, S. M., and Yu, J. Z.: Inter-comparison of NIOSH and IMPROVE protocols for OC and EC determination: implications for inter-protocol data conversion, *Atmos. Meas. Tech.*, 9, 4547-4560, <https://doi.org/10.5194/amt-9-4547-2016>, 2016.
- Wu, S. P., Cai, M. J., Xu, C., Zhang, N., Zhou, J. B., Yan, J. P., Schwab, J. J., and Yuan, C. S.: Chemical nature of PM_{2.5} and PM₁₀ in the coastal urban Xiamen, China: Insights into the impacts of shipping emissions and health risk, *Atmos. Environ.*, 227, <https://doi.org/10.1016/j.atmosenv.2020.117383>, 2020.

Yang, F., Tan, J., Zhao, Q., Du, Z., He, K., Ma, Y., Duan, F., Chen, G., and Zhao, Q.: Characteristics of PM_{2.5} speciation in representative megacities and across China, *Atmos. Chem. Phys.*, 11, 5207-5219, <https://doi.org/10.5194/acp-11-5207-2011>, 2011.

Yang, T., Chen, Y., Zhou, S., Li, H., Wang, F., and Zhu, Y.: Solubilities and deposition fluxes of atmospheric Fe and Cu over the Northwest Pacific and its marginal seas, *Atmos. Environ.*, 239, 117763, <https://doi.org/10.1016/j.atmosenv.2020.117763>, 2020.

Yen, P. -H., Yuan, C. -S., Ceng, J. -H., Chiang, K. -C., Tseng, Y. -L., Soong, K. -Y., and Jeng, M. -S.: Inter-comparison of chemical fingerprint and source apportionment of marine fine particles at two islands through the west and east passages of the Taiwan Island. *Sci. Total Environ.*, 851, 158313. <http://dx.doi.org/10.1016/j.scitotenv.2022.158313>, 2022.

Yen, P. -H., Yuan, C. -S., Wu, C. -H., Yeh, M. -J., Tseng, Y. -L., Soong, K. -Y.: Transport route-based cluster analysis of chemical fingerprints and source origins of marine fine particles (PM_{2.5}) in South China Sea. *Sci. Total Environ.*, 806, 150591. <https://doi.org/10.1016/j.scitotenv.2021.150591>, 2022.

Yuan, C. -S., Hung, C. -M., Hung, K. -N., Yang, Z. -M., Cheng, P. -H., and Soong, K. -Y.: Route-based chemical significance and source origin of marine PM_{2.5} at three remote islands in East Asia: Spatiotemporal variation and long-range transport. *Atmos. Pollut. Res.*, 14, 101762. <https://doi.org/10.1016/j.apr.2023.101762>, 2023.

Zhang, H., Li, R., Dong, S., Wang, F., Zhu, Y., Meng, H., Huang, C., Ren, Y., Wang, X., Hu, X., Li, T., Peng, C., Zhang, G., Xue, L., Wang, X., and Tang, M.: Abundance and Fractional Solubility of Aerosol Iron During Winter at a Coastal City in Northern China: Similarities and Contrasts Between Fine and Coarse Particles, *J. Geophys. Res.-Atmos.*, 127, <https://doi.org/10.1029/2021JD036070>, 2022.

Zhang, L., Gao, Y., Wu, S., Zhang, S., Smith, K. R., Yao, X., and Gao, H.: Global impact of atmospheric arsenic on health risk: 2005 to 2015, *P. Natl. Acad. Sci. USA*, 117, 13975-13982, <https://doi.org/10.1073/pnas.2002580117>, 2020.

Zhang, W., Peng, X., Bi, X., Cheng, Y., Liang, D., Wu, J., Tian, Y., Zhang, Y., and Feng, Y.: Source apportionment of PM_{2.5} using online and offline measurements of chemical components in Tianjin, China. *Atmos. Environ.*, 244, 117942. <https://doi.org/10.1016/j.atmosenv.2020.117942>, 2021.

Zhao, R., Han, B., Lu, B., Zhang, N., Zhu, L., and Bai, Z.: Element composition and source apportionment of atmospheric aerosols over the China Sea. *Atmos. Pollut. Res.*, 6, 191-201. <http://doi.org/10.5094/APR.2015.023>, 2015.

Zhu, Y., Li, W., Wang, Y., Zhang, J., Liu, L., Xu, L., Xu, J., Shi, J., Shao, L., Fu, P., Zhang, D., and Shi, Z.: Sources and processes of iron aerosols in a megacity in Eastern China, *Atmos. Chem. Phys.*, 22, 2191-2202. <https://doi.org/10.5194/acp-22-2191-2022>, 2022.